Ice Growth Acceleration by Antifreeze Proteins Leads to Higher Thermal Hysteresis Activity

Jinzi Deng, Elana Apfelbaum and Ran Drori*
Department of Chemistry and Biochemistry, Yeshiva University, New York, NY 10016, USA

Abstract

Since some antifreeze proteins and glycoproteins (AF(G)Ps) cannot directly bind to all crystal planes, they change ice crystal morphology by minimizing the area of the crystal planes to which they cannot bind until crystal growth is halted. Previous studies found that growth along the *c*-axis (perpendicular to the basal plane, the crystal plane to which these AF(G)Ps cannot bind) is accelerated by some AF(G)Ps, while growth of other planes is inhibited. The effects of this growth acceleration on crystal morphology and on the thermal hysteresis activity are unknown to date. Understanding these effects will elucidate the mechanism of ice growth inhibition by AF(G)Ps. Using cold stages and an Infrared laser, ice growth velocities and crystal morphologies in AF(G)P solutions were measured. Three types of effects on growth velocity were found: concentration-dependent acceleration, concentration-independent acceleration, and concentration-dependent deceleration. Quantitative crystal morphology measurements in AF(G)P solutions demonstrated that adsorption rate of the proteins to ice plays a major role in determining the morphology of the bipyramidal crystal. These results demonstrate that faster adsorption rates generate bipyramidal crystals with diminished basal surfaces at higher temperatures compared to slower adsorption rates. The acceleration of growth along the *c*-axis generates crystals with smaller basal surfaces at higher temperatures leading to increased growth inhibition of the entire crystal.

Introduction

Antifreeze proteins and glycoproteins (AF(G)Ps) protect organisms such as fish, plants and insects from freezing injuries in their cold environments by depressing the freezing temperature of extracellular ice[1–3]. This freezing point depression creates a temperature gap between the melting and freezing temperatures, known as thermal hysteresis (TH). AF(G)Ps have distinctive effects on the growth and melting of ice crystals, depending on their binding affinity to the ice crystal planes[4–6]. Most fish AF(G)Ps bind and inhibit prism, pyramidal, or both planes while incrementally decreasing the surface area of the basal plane[5,7,8]. This growth behavior results in a bipyramidal shaped crystal, of which the sharp tips indicate the narrowed basal plane. Therefore, the effectiveness of AF(G)Ps inhibition of crystal growth might be determined by how fast it minimizes the area of the basal plane to which they cannot bind. The competition between the adsorption rate of fish AF(G)Ps to prism and pyramidal planes and the advancing basal plane determines the TH activity[4,7,8] and affects crystal morphology. The ratio of the *c-to-a* axes is the quantitative measurement of crystal morphology[9,10], where the width of the bipyramidal crystal is measured along the *a*-axis and the length along the *c*-axis. These morphology measurements were done in different supercooling temperatures concentrations of AFP I and AFP III-QAE. With increasing concentrations of AFPIII-QAE a decreased *c-to-a* ratio was observed[10].

Another study investigated the effect of AFP mixtures on crystal morphology and TH activity by analyzing the *c-to-a* ratio, and found that this ratio changed mainly according to the crystal plane affinity of each AFP[9]. Several studies of ice growth velocity in the presence of fish AF(G)Ps have found that with increasing protein concentration, ice growth velocities along the *c*-axis increase[7,11,12]. AFPIII-QAE was

found to inhibit ice growth in both the crystallographic *a* and *c* directions at low supercoolings, and to accelerate growth at temperatures below a critical temperature, or burst point[11]. In these measurements, the AFPs were dissolved in pure water as opposed to buffer solutions with an adjusted pH value, which is the natural environment of AFPs. In another study that involved AFGPs, ice growth velocities were measured in $AFGP_{1-5}$ solutions using a glass tube immersed in a temperature-controlled bath[7]. Spicular growth of ice in temperatures between 0 °C and -2 °C was evident, and faster velocities were observed for higher AFGP concentrations. At these supercoolings, the ice growth velocity did not increase as the temperature decreased. Below -2 °C, dendritic growth was observed, and the clear trends described before, were not documented[7]. The smaller $AFGP_{7-8}$ was also able to accelerate the growth velocity along the *c*-axis. More recently, it was found that an AFP isolated from a diatom binds to the basal plane and inhibits the growth velocity along the *c*-axis[13].

To explain the accelerated growth in the presence of AF(G)Ps, it was proposed that the two-dimensional nucleation barrier is proportional to the decreased surface free energy of the solid-liquid interface[11,12]. With decreasing activation energy, the nucleation rate of new steps in the basal plane is increased. Another explanation included the transformation of crystal morphology to thinner dendrites, which gives rise to better latent heat dissipation[7,11]. This latent heat dissipation results in a higher growth velocity.

Weaver *et al*. observed similar crystal growth behavior with calcium oxalate monohydrate (COM) crystals in the presence of urinary proteins, such as Tamm-Horsfall glycoprotein (THP) and a synthetic 27-residue linear peptide[14]. They found that the kinetics of step growth on the basal plane was accelerated by the presence of THP but was inhibited by the linear peptide. To understand both the accelerated and inhibited growth velocities, they explained that aggregates of the peptides are associated with cation clouds that could contribute to a balance of charge[14]. The effect of AF(G)Ps on ice growth cannot be attributed to this reasoning because ice crystals lack an overall charge like COM. Additionally, there is evidence that AF(G)Ps do not form aggregates in solution[15].

It is unclear whether the effect of AF(G)Ps on growth velocity along the *c*-axis is correlated with their TH activity and a comparison between AF(G)Ps that accelerate ice growth was not completed to date. Here, we measured ice growth velocities in the presence of fish and plant AF(G)Ps and compared their TH activities to explain ice growth acceleration. Using light microscopy, cold stages and an IR laser, ice growth velocities along the *c*-axis of bipyramidal crystals in the presence of various AF(G)Ps were measured between the equilibrium melting point and the non-equilibrium freezing point (inside the hysteresis gap). The results were fit with an empirical equation and were correlated with binding planes, AF(G)P concentrations and TH activity. We found that although all AF(G)Ps inhibit growth along the *a*-axis, AFGPs accelerate growth along the *c*-axis in a concentration-independent manner, AFPs from fish (AFPIII-QAE and AFPI) accelerate growth in a concentration-dependent manner and an AFP from a ryegrass (*Lp*AFP) inhibits growth along both *a*- and *c*-axes.

Methods

Antifreeze proteins and glycoproteins

$AFGP_8$, $AFGP_{2,3,4}$ and AFPI were obtained as a gift from Konrad Meister and Arthur DeVries. AFPIII-QAE and *Lp*AFP were obtained as a gift from Peter Davies. $AFGP_8$ and $AFGP_{2,3,4}$ were diluted in double-distilled water, AFPIII-QAE and *Lp*AFP was diluted in 50mM Tris-HCL buffer (pH = 8) containing 100mM NaCl. More details on the proteins used in this study are presented in Table S1.

Ice growth velocity measurements and analysis

A custom-made cold stage mounted on an inverted microscope (Ti-S, Nikon, Japan), described previously[15,16], was used for these measurements along with a 980 nm IR laser (NaKu Technology, Hangzhou, China). First, a thin layer of immersion oil was applied onto the copper plate before a 1-inch diameter sapphire glass was placed on top. A three-microliter sample was pipetted onto the sapphire glass and covered with a smaller round cover glass with 1 cm-diameter, making a 20-30 µm layer of the AFP solution sandwiched between the sapphire disc and the glass cover slip. Then, a small amount of oil was applied around the edges of the cover glass to seal the openings so that the sample would not evaporate. A sCMOS (Neo, Andor, Ireland) was used for imaging and video analysis. Images and videos were analyzed using Nikon NIS-Elements software. After bipyramidal crystals were obtained (described in the results section), an IR laser (MDL-III-980, Opto Engin, Midvale, Utah, USA) was used to melt one tip of the crystal at various supercooling temperature (Fig. 1). At each supercooling temperature, the growth length of the melted tip was measured, and the time interval between the start and end of the growth was recorded. To fit the experimental results, an empirical equation used previously to describe ice growth was adopted (Eq. 1)[17–19]:

$$v = \alpha e^{\left(\frac{-\beta}{\Delta T}\right)} \qquad \text{(Eq. 1)}$$

where ΔT is the supercooling temperature (C), v is the ice growth velocity along the *c*-axis (µm/s), α (in units of µm/s) and β ((in units of °C) are empiric constants used to fit the experimental data. Data fitting was done by minimizing $\left(\frac{(v_{measured} - v_{calculated})}{\left(\frac{standard\ deviation}{v_{calculated}}\right)}\right)^2$ using the solver function in Microsoft Excel.

Results

Effects of AFP concentrations on ice growth velocities along the *c*-axis

The procedure of ice growth velocity measurements was initiated by cooling down to ~-20 °C to achieve ice nucleation. Then, the temperature was slowly increased until single bipyramidal-shaped crystals were obtained. These crystals were 15 - 30 µm in width. The melting temperature was then identified by fine tuning the temperature at a resolution of 0.001 °C. Next, the temperature was cooled and maintained at the desired supercooling temperatures and the tip of the crystal was melted using the IR laser as shown in Fig. 1B. When the IR laser was turned off, the ice growth along the *c*-axis (Fig. 1C) was observed and recorded. All measurements in this study were done on hexagonal bipyramids and at temperatures between the melting point of the crystal and its non-equilibrium freezing point (the temperature at which a burst growth is observed) point. For this reason, the concentrations of AF(G)Ps used here were limited and chosen based on the following constrains: at lower

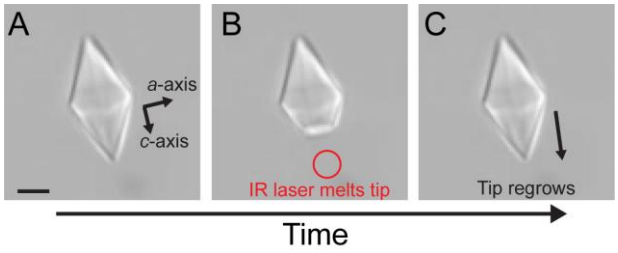

Fig. 1. Ice growth velocity measurements using an IR laser. In these experiments, the bottom crystal tip (A) is melted using an IR laser (B). Once the laser is turned off, ice growth immediately starts, and the tip is reformed (C). These measurements were conducted in various supercoolings and AFP concentrations. The ice velocity was measured after the experiments were completed using video analysis. Scale bar = 10 µm.

concentrations, a bipyramidal crystal was not formed, as the inhibition of the AF(G)P along the *a*-axis was not sufficient and growth in this direction was observed. On the other hand, if the AF(G)P concentration was too high, the crystals were small and rough and no bipyramidal crystals were observed. Another limitation of the higher concentrations was the availability of AF(G)Ps (mainly AFPI). Lastly, the measurements were also limited since the growth velocities in AFGPs solutions at supercooling degrees higher than 0.2-0.25 °C were around 150 µm/s, and our camera was not fast enough to capture the regrowth of the crystal tip. Thus, the range of concentrations and supercooling degrees that allowed the described measurements varied for each AF(G)P, which makes the comparison between AF(G)Ps more complicated.

At each supercooling temperature, the described procedure was performed at least 5 times. During all of our measurements, no growth was observed at supercooling temperatures lower than 0.04 °C. Ice growth velocities along the *c*-axis in AF(G)P solutions are shown in Figs. 2-4, and a combination of all tested AF(G)Ps is presented in Fig. 5, a summary of the AF(G)Ps information used in this study is presented in Table S1.

AFPIII-QAE and AFPI both exhibited accelerated growth velocities with higher AFP concentrations (indicated by the green arrow in Fig. 2A-2B). Note that the range of concentrations of AFPI that allowed bipyramidal growth velocity measurements was 10 times higher (by mass) than those of AFPIII-QAE (by molarity, the difference is up to 137 times higher for AFPI). For AFPI (3.3 kDa), growth velocities of 2 and 4 mg/ml were similar, and both were significantly lower than that of 6.5 mg/ml (Fig. 2A). For example, at 0.23 °C supercooling, the growth velocities were 6.8 and 6.4 µm/s for 2 and 4 mg/ml solutions, respectively, while the velocity in 6.5 mg/ml was almost 26 µm/s.

The ice growth velocities in AFPIII-QAE (7 kDa) solutions were comparable to the velocities measured at the low concentrations of AFPI (2 and 4 mg/ml), and about half the velocity measured for the highest AFPI concentration. Compared to AFPI, a clearer increase of the ice growth velocity with AFPIII-QAE concentration was observed (Fig. 2B). Clearly, both AFPI and AFPIII-QAE accelerate the growth of ice along the *c*-axis at a concentration-dependent manner.

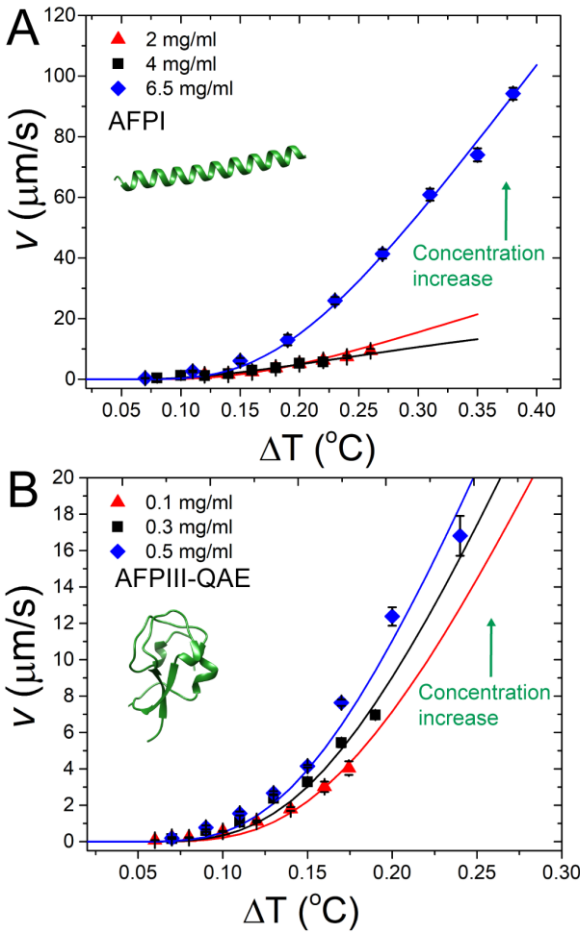

Fig. 2. Ice growth velocity along the *c*-axis in AFPI (A) and AFPIII-QAE (B) solutions. In both cases, the growth velocity increases with higher AFP concentrations (indicated by green arrow). Each data point contains at least 5 measurements, error bars indicate standard error. The data was fitted using Eq. 1. The fitting parameters are presented in Table S2.

Ice growth velocities in AFGP solutions were significantly higher (up to *20 times higher* at the same supercooling degree) than the velocities measured in AFPI and AFPIII-QAE solutions. In the presence of the smaller $AFGP_8$ (2.6 kDa), the growth velocity in a 1 mg/ml and 3 mg/ml were comparable (Fig. 3A). At a supercooling of 0.15 °C, the velocity reached 42

μm/s for 3 mg/ml, while the velocity in a 1 mg/ml solution was 54 μm/s at the same supercooling degree. The growth velocity in the presence of the bigger $AFGP_{2,3,4}$ (17 - 28.8 kDa) was comparable for 0.5 and 1 mg/ml at supercooling degrees lower than 0.15 °C (Fig. 3B). At lower temperatures, there seems to be higher velocities for the higher concentration (1 mg/ml). However, only 2 data points could be measured at supercooling degrees higher than 0.15 °C. Ice growth velocities in $AFGP_{2,3,4}$ solutions were slightly faster (~30%) than the velocity in $AFGP_8$ solutions, even though the molar concentrations of $AFGP_{2,3,4}$ used here (0.017 - 0.035 mM) were between one to two orders of magnitude lower than those of $AFGP_8$ (0.385 - 1.154 mM).

Deceleration of growth velocity at higher concentrations was observed in *Lp*AFP solutions (Fig. 4). At supercooling of 0.12 °C, the crystal growth velocity in a 0.5 mg/ml solution was 0.016 μm/s, twice that of 1 mg/ml. Note that growth velocities in *Lp*AFP solutions were 3 orders of magnitude slower compared to those measured in $AFGP_8$ solutions at similar supercoolings, which aligns well with the finding that this AFP binds to the basal plane[20].

Among all tested proteins, AFGPs achieved higher growth velocities than AFPs. As shown in Fig. 5, ice growth velocities in $AFGP_{2,3,4}$ and $AFGP_8$ solutions were faster by an order of magnitude compared by the velocities in AFPI and AFPIII-QAE solutions, which were faster by two orders of magnitude than the velocities in *Lp*AFP solutions. For example, at 0.15 °C supercooling, the growth velocity of 0.5 mg/ml $AFGP_{2,3,4}$ was more than 12-fold and 2500-fold higher than that of AFPIII-QAE and *Lp*AFP, respectively, at comparable molar concentrations.

The experimental measurements were described well by Eq. 1 (Figs. 2-5), with slight inaccuracies at low supercooling degrees (closer to the melting temperature). Note that in most cases, no growth was observed at these lower supercoolings (lower than 0.04 °C), however, these data points were not used to fit the experimental data using Eq. 1. For all AF(G)Ps except *Lp*AFP that inhibits growth along the *c*-axis, both α and β increased with concentration (see Table S2). In addition, the fit of the velocity measurements in *Lp*AFP solutions using Eq. 1 was not as good as the other proteins, suggesting slightly different mechanism.

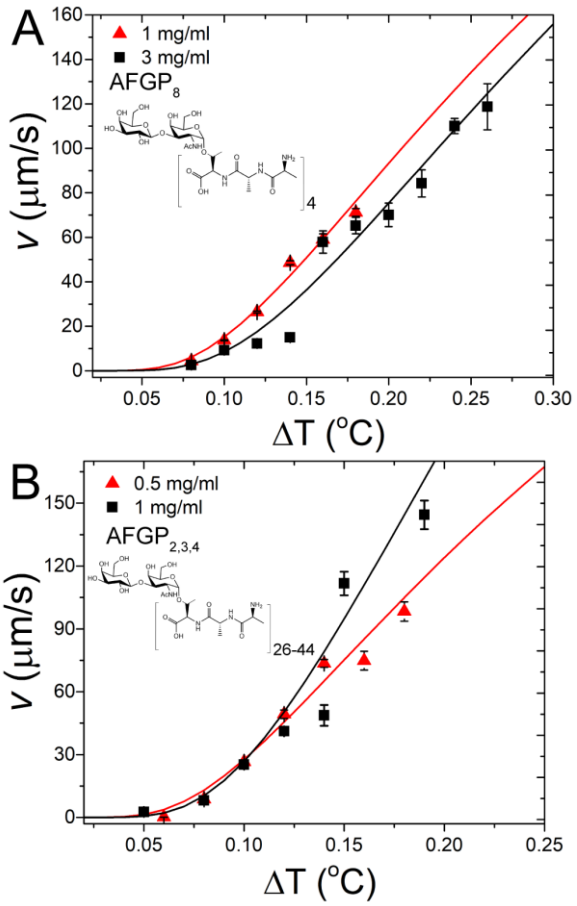

Fig. 3. Ice growth velocity along the *c*-axis in the presence of $AFGP_8$ (A) and $AFGP_{2,3,4}$ (B) at various concentrations. In both cases, there is no clear trend of the effect of AFGP concentration on growth velocity. Each data point contains at least 5 measurements, error bars indicate standard error. The data was fitted using Eq. 1. The fitting parameters are presented in Table S2.

Ice growth velocity along the *c*-axis and TH activity

AF(G)P concentrations play different roles on growth inhibition along the *a*-axis (Fig. 6, Data from reference[15]. Interestingly, the increase in TH activity seems to correlate with the acceleration along the *c*-axis. AFPIII-QAE, $AFGP_{2,3,4}$ and AFPI obtained higher TH activity compared to *Lp*AFP and both proteins accelerate growth velocity along the *c*-axis as well. On the contrary, *Lp*AFP decelerates the growth velocity along the *c*-axis but did not inhibit the growth along *a*-axis as well as the other proteins. In other words, with increasing concentrations, AFPIII-QAE and AFPI have a greater inhibition effect along the *a*-axis while accelerating the growth velocity along the *c*-axis.

$AFGP_{2,3,4}$ did not have a clear trend of concentration effect on ice growth velocity. The TH activity of $AFGP_8$ is known to be lower than the other fish AF(G)Ps tested here[21–23], however, it was not measured for this protein since the crystal burst is different compared to other AF(G)Ps. As the temperature is decreased, crystals in the presence of $AFGP_8$ grew along the *c*-axis while growth along the *a*-axis remains stagnant. This behavior results in elongated crystals, comparable to the needle-like crystals observed in the presence of safranine O[24]. Thus, the definition of 'crystal burst' becomes different for $AFGP_8$ compared to the rest of the AF(G)Ps and TH activity of this protein was not included in this study.

We observed that the TH activity of *Lp*AFP (1 mg/ml) increased with higher exposure time of the crystal to the AFP solution (also termed annealing time by others[25]) (Fig. 7). In these experiments, the crystal is held at a constant temperature for various time periods before cooling towards the freezing temperature[4,25].

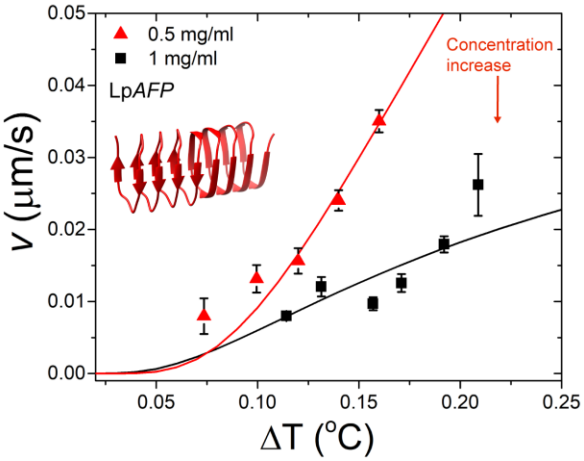

Fig. 4. Ice growth velocity along the *c*-axis in the presence of *Lp*AFP at two concentrations. The growth velocity decreases with higher AFP concentrations (indicated by red arrow). Each data point contains at least 5 measurements, error bars indicate standard error. The data was fitted using Eq. 1. The fitting parameters are presented in Table S2.

The TH activity increased from 0.206 °C at an exposure time of 18 seconds, to 0.28 °C after exposing the crystal to *Lp*AFP solution for 120 minutes. The crystals that were exposed to the *Lp*AFP solution for short times (<=1 minute) exhibited a burst that was initiated at the prism plane (Fig. 7, left). This burst looked like a widening of the crystal and growth along the *a*-axis. However, at long exposure times (>10 minutes) the crystals were shaped as bipyramids and the burst was always initiated at the crystal tips, which are basal plane surfaces (Fig. 7, right). Thus, these results demonstrate how crystal morphology affects TH activity. Next, crystal morphology was measured, and the effect of adsorption rate of AF(G)Ps was investigated.

Quantifying crystal morphology according to adsorption rates

The dimensions of bipyramidal crystals in $AFGP_{1-5}$ and AFPIII-QAE were measured at various concentrations. These proteins were chosen since their adsorption rate is known[4,16]. After isolating single crystals, the temperature was slowly decreased (0.075 °C/min) and at some point, the pyramidal planes converged into sharp tips. The temperature was lowered at the above rate until crystal burst was observed. Using video analysis, the last frame before the crystal burst was used to measure the crystal dimensions and

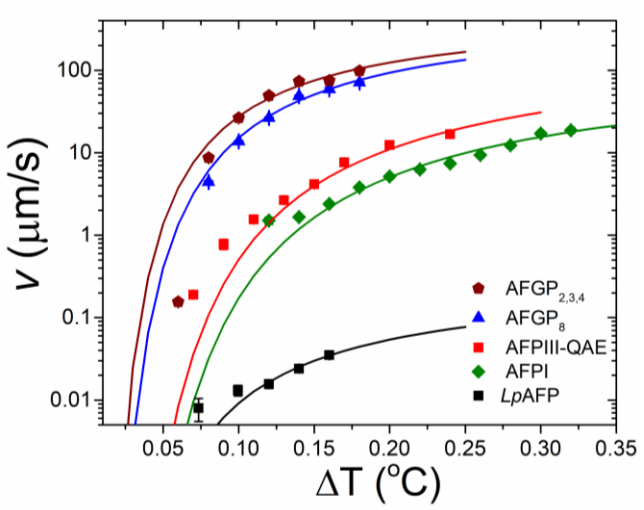

Fig. 5. Ice growth velocity (on a logarithmic scale) along the *c*-axis in the presence of all AF(G)Ps tested at the following concentrations: ***Lp*AFP**, 0.5 mg/ml or 0.037 mM. **$AFGP_8$**, 1 mg/ml or 0.385 mM. **AFPI**, 2 mg/ml or 0.606 mM. **AFPIII-QAE**, 0.5 mg/ml or 0.071 mM. **$AFGP_{2,3,4}$**, 0.5 mg/ml or 0.017 - 0.029 mM (this AFGP is a mixture of AFGPs at molecular weights of 28.8 - 17 kDa).

to obtain the c-to-a ratio. This ratio is between the length of the crystal (from tip to tip) along the *c*-axis and the width of the crystal along the *a*-axis[9,10]. In the case of $AFGP_{1-5}$, spicules that grew along the *c*-axis were not considered in the measurement.

The adsorption rate of AF(G)Ps includes two components: [1] the intrinsic adsorption rate of each protein (k_{on}) and [2] the concentration (c) of that protein in solution[4,16]. A clear correlation was found (Fig. 8) between the adsorption rates ($k_{on}c$) of $AFGP_{1-5}$/AFPIII-QAE and the *c-to-a* ratio. Our measurements (black squares) contain $AFGP_{1-5}$/AFPIII-QAE, while measurements done by the Davies group[10] (red circles) included crystals in AFPIII-QAE solutions. At low adsorption rates the crystals were more elongated (higher *c-to-a* ratio), and as the adsorption rate increases, the *c-to-a* ratio decreases until it plateaus at ~1.7. The data points in Fig. 8 consist of crystals in $AFGP_{1-5}$ and AFPIII-QAE, suggesting that the effect of adsorption rate on crystal morphology is similar for these two proteins, although AFPIII-QAE binds to pyramidal planes and it is unclear whether $AFGP_{1-5}$ also binds to these planes.

Discussion

The intriguing phenomenon involving AF(G)Ps that inhibit the growth along the *a*-axis while accelerating the growth along the *c*-axis was studied here. Based on our experimental results, we hypothesize that there are three types of relationships between AF(G)P concentration and the ice growth velocity within the hysteresis gap. First, for $AFGP_8$ and $AFGP_{2,3,4}$, higher protein concentrations do not seem to cause an increased ice growth velocity. Second, for *Lp*AFP, higher protein concentration led to lower growth velocities. Last, for AFPI and AFPIII-QAE, higher protein concentrations increased growth velocities.

Eq. 1 that was used to fit the experimental measurements indicated that both fitting constants, α and β, change with protein concentration. However, more experiments and simulations are needed to draw conclusions from the physical meaning of these constants, which probably contain a few parameters for each constant. Previous ice growth velocity measurements agreed with this type of function

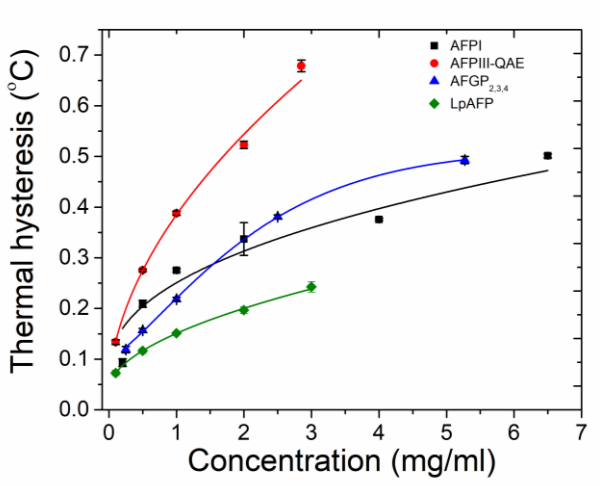

Fig. 6. TH activity of the AF(G)Ps tested here. Data from reference 15.

without AFPs[17,19] or in the presence of AFPs[18]. The latter suggested that 2D step nucleation mechanism[18] is described well by exp(-1/ΔT), which is the mechanism that describes growth along the *c*-axis[7,17].

Although the fitting constants, α and β, increased with AFGP concentrations (both $AFGP_{2,3,4}$ and $AFGP_8$), the growth velocities were similar for the tested concentrations. This indicates that for AFGPs at the concentrations tested here, higher concentration did not affect the growth velocity, but faster velocities were obtained at higher supercoolings. This result contrasts with a previous study[7], which found significant increase in growth velocity with $AFGP_{1-5}$ concentrations. These researchers found no significant increase in growth velocity at supercooling degrees lower than -2 °C (at temperatures between the melting point and -2 °C). These discrepancies are a result of different phenomena - the current study measured growth velocities in the hysteresis gap while Knight and DeVries[7] measured the growth velocities of spicules that occur only after the growth burst (below the freezing temperature). Still, ice growth velocities along the *c*-axis in AFGP solutions were found to be faster than other AFPs by an order of magnitude.

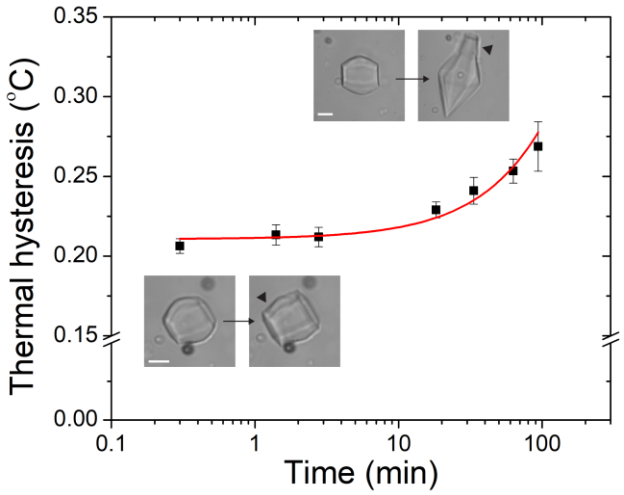

Fig. 7. TH activity and crystal morphology in a 1 mg/ml *Lp*AFP solution. Black arrows in inserts indicate the location at which the growth burst started. At short exposure times, sharp tips were not formed before the crystal burst (bottom insert). At higher exposure times (>10 minutes) sharp tips were formed, the TH activity increased, and the growth burst initiated at the tip of the crystal. Each data point represents 5 crystals and error bars indicate standard error. Scale bar = 10 µm.

When the concentration of *Lp*AFP was increased by a factor of 2, a clear deceleration (or inhibition) of growth velocity along *c*-axis was observed. *Lp*AFP is the only protein tested here that binds to the basal plane[20], which indeed provides effective inhibition of the growth velocity along the *c*-axis compared to the other AF(G)Ps tested here. Even though *Lp*AFP binds to the basal plane, a bipyramidal crystal is observed in the presence of this AFP. Usually, AFPs that bind to the basal plane induce a lemon-shaped crystal[5] rather than a bipyramidal crystal. *Lp*AFP is unique in the sense that it inhibits growth along the *c*-axis, but not enough to induce a lemon-shaped ice crystal. The TH activity of *Lp*AFP is lower than that of AFPIII-QAE, AFPI and $AFGP_{2,3,4}$, which may be due to a lower adsorption rate of *Lp*AFP compared to the other proteins. This is supported by our previous finding that TH activity and adsorption rates are correlated[16].

The effect of exposure time on TH activity of *Lp*AFP was comparable to that of AFPIII-QAE[4,25]. At supercooling temperature of 0.15 °C, after exposure times of up to 120 minutes to *Lp*AFP solutions, the TH activity increased 1.4-fold, indicating a higher inhibition effect with extended exposure times. The TH activity of insect and bacterial AFPs (*Tm*AFP, sbwAFP and *Mp*AFP) increased by up to 40-fold with extended exposure times[4]. These AFPs bind to the basal plane and slowly accumulate on this surface. In contrast, the TH activity of AFPIII-QAE increased 1.5[4] to 2.5-fold[25] at exposure times of 60 and 180 minutes, respectively. The TH increased most significantly when the crystal was exposed to AFPIII-QAE solutions at high supercooling degrees. As AFPIII-QAE cannot bind to the basal plane and its accumulation on the prism plane saturates within minutes[4], the increased TH with extended exposure time stems from the

decreased area of the basal plane[7,8]. In contrast, *Lp*AFP that accumulates on the prism and basal planes, probably exhibits both effects described above; it slowly accumulates on the basal plane and the area of the basal plane decreases with extended exposure times.

It seems reasonable to suggest that the ability of *Lp*AFP to bind to the basal plane, does not provide higher TH activity, as was suggested recently for a diatom AFP[13]. However, freeze-tolerant plants mainly require ice recrystallization inhibition (IRI)[26], and the ability to bind to multiple crystal planes might be key to obtain higher IRI activity[27]. The crystal structure of a carrot AFP (*Dc*IBP) was recently solved and while its structure is different compared to that of *Lp*AFP, both plant AFPs exhibit low TH activity and high IRI activity[28].

Crystal morphology was also found to be well correlated with adsorption rates. Faster adsorption rate of the inhibitor to prism planes generates shorter risers (or steps) and larger terraces (shown schematically in Fig. 9). Thus, when comparing two AF(G)Ps with slow and fast adsorption rates, the number of risers needed to obtain a small basal surface is fewer for the protein with the faster adsorption rate. Assuming that riser height is the same for both cases, a bipyramidal crystal in the presence of an AF(G)P with a slow adsorption rate will require more risers to form a terrace similar in size and small enough to slow down step nucleation on that basal surface. Higher concentrations of AFPIII-QAE and AFPI accelerated ice growth velocity and both α and β increased with higher AFP concentrations, although a decrease of α and β was observed for AFPI at 4 mg/ml compared to 2 mg/ml. In this category, both proteins bind to the pyramidal plane (AFPIII-QAE also binds to the prism plane) and prevent growth of these faces[6,29].

Binding to pyramidal planes may generate new source of growth steps and promote the growth velocity along the basal plane. A similar hypothesis has been postulated by Furukawa *et al.*[12,30], although their theory involved AFGP molecules, which preferentially adsorb to the prismatic plane. A higher level of acceleration by AFPI compared to AFPIII-QAE was observed. However, the concentration of AFPIII-QAE used here was an order of magnitude lower than that of AFPI (by mass) to allow the formation of bipyramidal crystals.

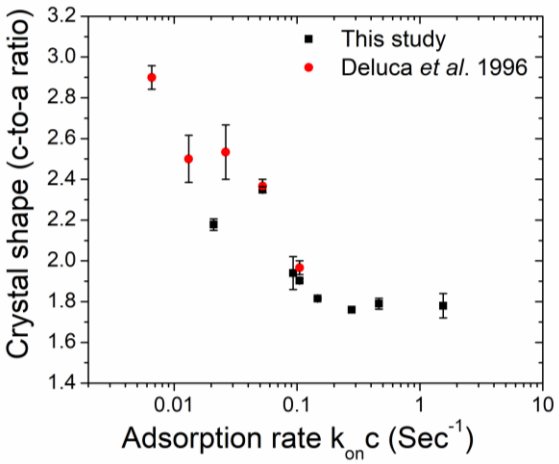

Fig. 8. Crystal shape in $AFGP_{1-5}$ and AFPIII-QAE solutions were measured as the ratio between the length of the crystal (along the *c*-axis) and the width (along the *a*-axis). The intrinsic adsorption rates, k_{on}, of $AFGP_{1-5}$ = 0.31 mg mL^{-1} sec^{-1} and the k_{on} of AFPIII-QAE = 0.21 mg mL^{-1} sec^{-1}. Black data points represent data from this study, red data points represent data from reference 10.

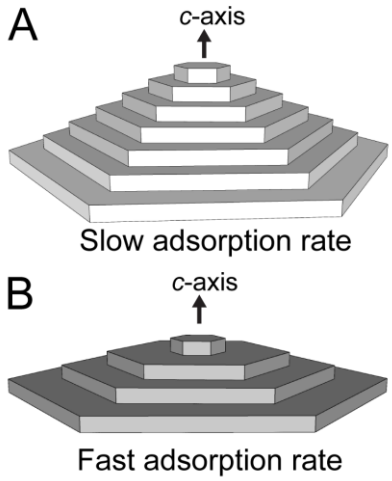

Fig. 9. Schematic description of the effect of adsorption rate on crystal morphology. An AF(G)P with slow adsorption rate will generate longer risers and smaller terraces (A) compared to an AF(G)P with fast adsorption rate (B). Thus, more steps are needed to obtain the tip of the pyramid in A. Note that the smallest terrace on top and the largest terrace at the bottom have the same dimensions in A and B.

The effects of AF(G)Ps on growth velocity along the *c*-axis might be correlated to TH activity. The AF(G)Ps that were found to accelerate growth along the *c*-axis, AFPIII-QAE, AFPI and $AFGP_{2,3,4}$ exhibit higher TH activity than *Lp*AFP, which inhibits growth along the *c*-axis. One possible need for growth acceleration along the *c*-axis, is to minimize the area of the basal plane of the crystal by converging the pyramidal planes. In this scenario, the bipyramidal crystal would form its tips at lower supercooling degrees compared to an AF(G)P that does not accelerate the growth along the *c*-axis, for example *Lp*AFP. Thus, the basal plane area to which the AF(G)Ps cannot bind (except *Lp*AFP) is minimized, and the "weak" points of the crystal are eliminated. This possibility might explain the low TH activity of *Lp*AFP compared to the other AF(G)Ps tested here.

Conclusions

AF(G)Ps have different abilities to affect ice growth due to various degrees of affinity for binding planes and adsorption rates. By comparing $AFGP_8$, $AFGP_{2,3,4}$, *Lp*AFP, AFPI and AFPIII-QAE, we demonstrated the wide range of acceleration/deceleration of ice growth velocity along the *c*-axis. We revealed three categories of ice growth acceleration along the *c*-axis: AFGPs accelerate the growth in a concentration-independent manner, *Lp*AFP inhibits growth in a concentration-dependent manner, and AFPI and AFPIII-QAE accelerate the growth along the *c*-axis with higher concentrations. The growth inhibition along the *a*-axis, measured by TH activity, is more uniform across the board and increases with higher concentrations for all AF(G)Ps. The acceleration of ice growth along the *c*-axis benefits AF(G)Ps by obtaining sharper bipyramidal tips and thus smaller basal surface at higher temperatures, thereby eliminating the crystal plane that is not inhibited by adsorption. Future experiments and simulations will reveal the molecular mechanism of ice growth acceleration and the physical meaning of the fitting constants (α and β) used here.

Supporting Information

Table S1 - AF(G)Ps tested in this study.
Table S2 - Fitting constants α and β for each protein.

***- corresponding author** - rdrori@yu.edu.

Acknowledgments

The authors thank Prof. Peter Davies for sharing *Lp*AFP and AFPIII-QAE samples, Dr. Konrad Meister and Prof. Arthur DeVries for sharing the AFGPs and AFPI. The authors also thank Nechama Dembitzer and Nicole Soussana for data collection.

References

(1) DeVries, A. L.; Komatsu, S. K.; Feeney, R. E. Chemical and Physical Properties of Freezing Point-Depressing Glycoproteins from Antarctic Fishes. *J. Biol. Chem.* **1970**, *245* (11), 2901–2908.
(2) Evans, C. W.; Gubala, V.; Nooney, R.; Williams, D. E.; Brimble, M. A.; Devries, A. L. How Do Antarctic Notothenioid Fishes Cope with Internal Ice? A Novel Function for Antifreeze Glycoproteins. *Antarct. Sci.* **2010**, *23* (1), 57–64.
(3) Bar Dolev, M.; Braslavsky, I.; Davies, P. L. Ice-Binding Proteins and Their Function. *Annu. Rev. Biochem.* **2016**, *85*, 515–542.
(4) Drori, R.; Celik, Y.; Davies, P. L.; Braslavsky, I. Ice-Binding Proteins That Accumulate on Different Ice Crystal Planes Produce Distinct Thermal Hysteresis Dynamics. *J. R. Soc. Interface* **2014**, *11* (98), 20140526.

(5) Bar-Dolev, M.; Celik, Y.; Wettlaufer, J. S.; Davies, P. L.; Braslavsky, I. New Insights into Ice Growth and Melting Modifications by Antifreeze Proteins. *J. R. Soc. Interface* **2012**, *9* (77), 3249–3259.
(6) Basu, K.; Garnham, C. P.; Nishimiya, Y.; Tsuda, S.; Braslavsky, I.; Davies, P. Determining the Ice-Binding Planes of Antifreeze Proteins by Fluorescence-Based Ice Plane Affinity. *J. Vis. Exp.* **2014**, (83):e51185.
(7) Knight, C. A.; DeVries, A. L. Ice Growth in Supercooled Solutions of a Biological "Antifreeze", AFGP 1-5: An Explanation in Terms of Adsorption Rate for the Concentration Dependence of the Freezing Point. *Phys. Chem. Chem. Phys.* **2009**, *11* (27), 5749–5761.
(8) Drori, R.; Davies, P. L.; Braslavsky, I. When Are Antifreeze Proteins in Solution Essential for Ice Growth Inhibition? *Langmuir* **2015**, *31* (21), 5805–5811.
(9) Heman, C.; DeLuca, C. I.; Davies, P. L. Mixing Antifreeze Protein Types Changes Ice Crystal Morphology without Affecting Antifreeze Activity. *FEBS Lett.* **1995**, *357* (2), 183–186.
(10) DeLuca, C. I.; Chao, H.; Sönnichsen, F. D.; Sykes, B. D.; Davies, P. L. Effect of Type III Antifreeze Protein Dilution and Mutation on the Growth Inhibition of Ice. *Biophys. J.* **1996**, *71* (5), 2346–2355.
(11) Vorontsov, D. A.; Sazaki, G.; Titaeva, E. K.; Kim, E. L.; Bayer-Giraldi, M.; Furukawa, Y. Growth of Ice Crystals in the Presence of Type III Antifreeze Protein. *Cryst. Growth Des.* **2018**, *18* (4), 2563–2571.
(12) Furukawa, Y.; Nagashima, K.; Nakatsubo, S. I.; Yoshizaki, I.; Tamaru, H.; Shimaoka, T.; Sone, T.; Yokoyama, E.; Zepeda, S.; Terasawa, T.; et al. Oscillations and Accelerations of Ice Crystal Growth Rates in Microgravity in Presence of Antifreeze Glycoprotein Impurity in Supercooled Water. *Sci Rep* **2017**, *7*, 43157.
(13) Bayer-Giraldi, M.; Sazaki, G.; Nagashima, K.; Kipfstuhl, S.; Vorontsov, D. A.; Furukawa, Y. Growth Suppression of Ice Crystal Basal Face in the Presence of a Moderate Ice-Binding Protein Does Not Confer Hyperactivity. *Proc. Natl. Acad. Sci.* **2018**, *115* (29), 7479–7484.
(14) Weaver, M. L.; Qiu, S. R.; Hoyer, J. R.; Casey, W. H.; Nancollas, G. H.; De Yoreo, J. J. Surface Aggregation of Urinary Proteins and Aspartic Acid-Rich Peptides on the Faces of Calcium Oxalate Monohydrate Investigated by In Situ Force Microscopy. *Calcif. Tissue Int.* **2009**, *84* (6), 462–473.
(15) Berger, T.; Meister, K.; DeVries, A. L.; Eves, R.; Davies, P. L.; Drori, R. Synergy between Antifreeze Proteins Is Driven by Complementary Ice-Binding. *J. Am. Chem. Soc.* **2019**, *141* (48), 19144–19150.
(16) Meister, K.; DeVries, A. L.; Bakker, H. J.; Drori, R. Antifreeze Glycoproteins Bind Irreversibly to Ice. *J. Am. Chem. Soc.* **2018**, *140*, (30), 9365-9368.
(17) Hobbs, P. V. *Ice Physics*; Clarendon, Oxford, 1974.
(18) Inada, T.; Koyama, T.; Funakoshi, K. Pit Formation on the Basal Plane of Ice in Antifreeze Protein Type III Solution for Different Growth Mechanisms of Ice. *Cryst. Growth Des.* **2016**, *16* (7), 3587–3595.
(19) Wilen, L. A.; Dash, J. G. Giant Facets at Ice Grain Boundary Grooves. *Science.* **1995**, *270* (5239), 1184–1186.
(20) Middleton, A. J.; Marshall, C. B.; Faucher, F.; Bar-Dolev, M.; Braslavsky, I.; Campbell, R. L.; Walker, V. K.; Davies, P. L. Antifreeze Protein from Freeze-Tolerant Grass Has a Beta-Roll Fold with an Irregularly Structured Ice-Binding Site. *J. Mol. Biol.* **2012**, *416* (5), 713–724.
(21) Knight, C. A; DeVries, A. L.; Oolman, L. D. Fish Antifreeze Protein and the Freezing and Recrystallization of Ice. *Nature* **1984**, *308* (5956), 295–296.
(22) Meister, K.; Duman, J. G.; Xu, Y.; DeVries, A. L.; Leitner, D. M.; Havenith, M. The Role of Sulfates on Antifreeze Protein Activity. *J. Phys. Chem. B* **2014**, *118* (28), 7920–7924.
(23) Tachibana, Y.; Fletcher, G. L.; Fujitani, N.; Tsuda, S.; Monde, K.; Nishimura, S. I. Antifreeze Glycoproteins: Elucidation of the Structural Motifs That Are Essential for Antifreeze Activity. *Angew. Chemie-International Ed.* **2004**, *43* (7), 856–862.

(24) Drori, R.; Li, C.; Hu, C.; Raiteri, P.; Rohl, A. L.; Ward, M. D.; Kahr, B. A Supramolecular Ice Growth Inhibitor. *J. Am. Chem. Soc.* **2016**, *138* (40), 13396–13401.
(25) Takamichi, M.; Nishimiya, Y.; Miura, A.; Tsuda, S. Effect of Annealing Time of an Ice Crystal on the Activity of Type III Antifreeze Protein. *FEBS J.* **2007**, *274* (24), 6469–6476.
(26) Sidebottom, C.; Buckley, S.; Pudney, P.; Twigg, S.; Jarman, C.; Holt, C.; Telford, J.; McArthur, A.; Worrall, D.; Hubbard, R.; et al. Heat-Stable Antifreeze Protein from Grass. *Nature* **2000**, *406* (6793), 256.
(27) Rahman, A. T.; Arai, T.; Yamauchi, A.; Miura, A.; Kondo, H.; Ohyama, Y.; Tsuda, S. Ice Recrystallization Is Strongly Inhibited When Antifreeze Proteins Bind to Multiple Ice Planes. *Sci. Rep.* **2019**, *9* (1), 2212.
(28) Wang, Y.; Graham, L. A.; Han, Z.; Eves, R.; Gruneberg, A. K.; Campbell, R. L.; Zhang, H.; Davies, P. L. Carrot 'Antifreeze' Protein Has an Irregular Ice-Binding Site That Confers Weak Freezing Point Depression but Strong Inhibition of Ice Recrystallization. *Biochem. J.* **2020**, *477* (12), 2179–2192.
(29) Knight, C. A.; Cheng, C. C.; DeVries, A. L. Adsorption of Alpha-Helical Antifreeze Peptides on Specific Ice Crystal Surface Planes. *Biophys. J.* **1991**, *59* (2), 409–418.
(30) Furukawa, Y.; Nagashima, K.; Nakatsubo, S.; Zepeda, S.; Murata, K. I.; Sazaki, G. Crystal-Plane-Dependent Effects of Antifreeze Glycoprotein Impurity for Ice Growth Dynamics. *Philos. Trans. R. Soc. A Math. Phys. Eng. Sci.* **2019**, *377* (2146).